DC Capacitance Reduction in Three-Phase Photovoltaic Inverters by using Virtual Impedance Emulation

Andoni Urtasun, Pablo Sanchis and Luis Marroyo
Department of Electrical and Electronic Engineering
Institute of Smart Cities
Public University of Navarre (UPNA)
Pamplona, Spain

Acknowledgments

This work was supported by the Spanish State Research Agency (AEI) and FEDER-UE under grant DPI2016-80641-R. The authors gratefully acknowledge the financial and ongoing support of INGETEAM POWER TECHNOLOGY.

Keywords

«Converter control», «Frequency-Domain Analysis», «Photovoltaic», «Renewable energy systems».

Abstract

DC voltage regulation in grid-connected three-phase PV inverters is a fundamental requirement. In order to reduce the influence of the PV non-linear behavior and ensure stability in the whole operating range, the input capacitance in high-power inverters is currently oversized, thus increasing the converter cost. This paper proposes a control method which emulates a virtual impedance in parallel with the PV generator, making it possible to reduce the capacitance by a factor of 5. Simulation results confirm that the proposed control is stable and fast enough in the whole operating range with such a small capacitor.

1. Introduction

Photovoltaic (PV) capacity is growing very quickly thanks to its increasingly competitive prices. In 2017, at least 98 GWp of solar PV power was installed, increasing total capacity by nearly one-third, for a cumulative total of approximately 402 GWp [1].

In order to deliver its power to the grid, the PV generator can be interfaced by a three-phase inverter, which is usually connected to the grid through an LCL filter, as shown in Fig. 1 [2], [3]. The input voltage control is carried out by means of a cascaded regulation, where the outer loop obtains the active power reference to be injected into the grid.

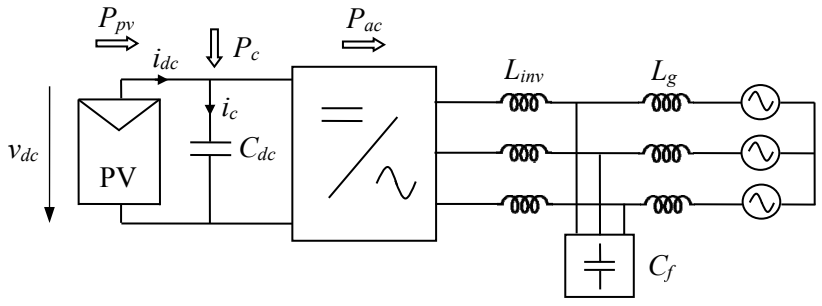

Fig. 1: Three-phase photovoltaic inverter connected to the grid.

Traditionally, the input capacitor has been considered as the plant for the voltage regulation, not taking into account the PV generator influence [4]. However, in the last years it has been shown that the PV non-linear behavior can have large impact on the control, especially when using small capacitors and low crossover frequencies [5]–[7]. In the case of PV inverters, the open-loop transfer function of the dc voltage regulation strongly depends on the operating point, and a Right-Half-Plane (RHP) pole appears when the PV voltage is below the Maximum Power Point (MPP) voltage [8]. Although this operating point is not desired, the system can end up in this situation after an irradiance drop or a misled MPPT. In this situation, in order to ensure stability, the crossover frequency should be at least two times higher than the frequency of the RHP pole [9]. However, to reject the second harmonic in the dc voltage inherent to unbalanced grids (especially significant during asymmetric voltage sags), the crossover frequency is limited to 10–15 Hz. For this reason, the input capacitance must often be oversized in order to reduce the RHP pole frequency and then guarantee voltage control stability [10].

This paper proposes a voltage control method which makes it possible to reduce the input capacitance, therefore reducing the converter cost and size. For this purpose, first the inner power loop is modified in order to emulate a virtual impedance which removes the RHP pole from the plant seen by the voltage controller. Then, once the RHP pole is eliminated, the voltage controller can be readily designed.

2. System Modeling

The voltage regulation scheme is shown in Fig. 2, where v^*_{dc} is the reference dc voltage, $v_{dc,f}$ the measured and filtered dc voltage, P^*_{ac} the reference power, C represents the controller, D the digital sampling, computation and Zero-Order Hold (ZOH) delays, G_{cl} the inner closed-loop, Z_c the capacitor impedance, H the analog voltage filter and DSC the delayed signal cancellation, used to remove the second harmonic present in the dc voltage. As can be observed, the square of the voltage is the control variable and the controller obtains the active power to be injected to the grid. Then, this power will be regulated by means of two current loops, either in stationary or synchronous reference frame.

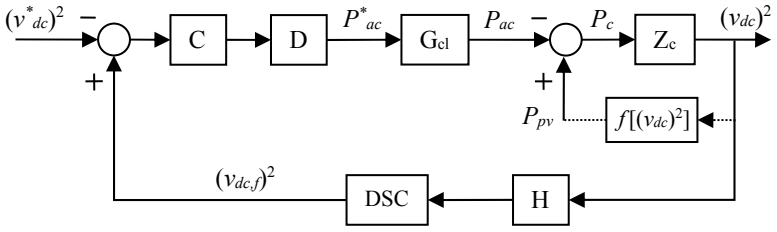

Fig. 2: Control loop for the conventional voltage regulation.

The power flowing through the input capacitor, P_c, and the capacitor impedance transfer function in Laplace domain, $Z_c(s)$, can be expressed as

$$P_c = v_{dc} \cdot i_c = C_{dc} \cdot v_{dc} \cdot \frac{dv_{dc}}{dt} = \frac{C_{dc}}{2} \cdot \frac{dv_{dc}^2}{dt} \quad \Rightarrow \quad Z_c(s) = \frac{v_{dc}^2}{P_c} = \frac{2}{C_{dc} \cdot s}. \tag{1}$$

If the PV generator is disregarded, (1) represents the system plant. However, in reality the PV power is dependent on $(v_{dc})^2$ (see Fig. 2), and therefore has an effect on the actual plant. To quantify this influence, a small-signal linearization of the generator P–V curve is carried out:

$$\hat{P}_{pv} = \left.\frac{\partial P_{pv}}{\partial v_{dc}}\right|_{V_{dc},I_{dc}} \cdot \hat{v}_{dc} = \frac{1}{2 \cdot V_{dc}} \cdot \left.\frac{\partial P_{pv}}{\partial v_{dc}}\right|_{V_{dc},I_{dc}} \cdot \hat{v}_{dc}^2, \tag{2}$$

where V_{dc} and I_{dc} are the PV generator voltage and current at the operating point.

From (2), it can be deduced that the P–V curve slope is crucial for small-signal stability. In particular, when the operating voltage is above MPP, the slope is negative and the PV generator behaves as a positive resistance/conductance; if the voltage is equal to MPP voltage, the slope is zero and the generator has no influence on the control; finally, when the voltage is below MPP, the slope is positive and the generator behaves as a negative resistance/conductance. In the latter situation, a decrease in the dc voltage causes a reduction of the PV power delivered, contributing towards instability.

Since $P_{pv} = v_{dc} \cdot i_{dc}$, from (2),

$$\hat{P}_{pv} = -\frac{1}{2} \cdot \left(-\frac{\partial i_{dc}}{\partial v_{dc}} - \frac{I_{dc}}{V_{dc}} \right) \cdot \hat{v}_{dc}^2 = -\frac{g_{pv} - g_0}{2} \cdot \hat{v}_{dc}^2 = -\frac{g_t}{2} \cdot \hat{v}_{dc}^2 \tag{3}$$

$$g_t = g_{pv} - g_0, \quad g_{pv} = -\frac{\partial i_{dc}}{\partial v_{dc}}, \quad g_0 = \frac{I_{dc}}{V_{dc}}, \tag{4}$$

where g_{pv} is the dynamic conductance of the PV generator, g_0 its static conductance, and g_t its total conductance. While g_{pv} and g_0 are always positive, g_t is positive above MPP voltage and negative below MPP voltage.

Integrating the PV generator model into the system plant (see Fig. 2), the P_{ac} to $(v_{dc})^2$ transfer function also depends on the total conductance g_t. On account of (1) and (3), one obtains

$$Z_{c,pv}(s) = -\frac{\hat{v}_{dc}^2}{\hat{P}_{ac}} = \frac{2}{C_{dc} \cdot s + g_t} \quad \Rightarrow \quad \omega_p = -\frac{g_t}{C_{dc}}, \tag{5}$$

where ω_p is the pole frequency.

Thus, when operating with a voltage above MPP ($g_t > 0$), the pole is in the Left-Half-Plane (LHP), whereas it lies in the RHP for a voltage below MPP ($g_t < 0$). It is worth noting that the same pole appears for both v_{dc} [10] and v_{dc} square controls since it is related to the same physical phenomenon, a finite power source interfaced by a current-controlled inverter, which behaves as a constant power load.

From (5), it can be observed that the PV array effect is more important at low frequencies, for small input capacitors and for high total conductance g_t. For this reason, it is particularly significant for high-power central inverters, where the PV generator can even reach 2 or 3 kA at low voltage, resulting in high g_t values. In these converters, since the crossover frequency ω_c is restricted, the dc capacitor is presently oversized in order to reduce the PV array influence.

For a correct dc capacitor sizing, it is thus important to quantify the PV array influence, which can be realized by determining the total conductance boundaries. Its minimum value is especially relevant since could lead to instability. On account on the PV inverter current and voltage ratings, the minimum total conductance can be obtained as [10]

$$g_{t,\min} = \left(g_{pv} - g_0 \right)_{\min} \approx -g_{0,\max} = -\frac{I_{sc,\max}}{V_{dc,\min}}, \tag{6}$$

where $I_{sc,max}$ is the maximum short-circuit current in Standard Test Conditions (STC), and $V_{dc,min}$ is the minimum dc voltage, which depends on the grid rms voltage.

3. Conventional Voltage Regulation

The conventional voltage regulation scheme, now including the obtained system plant (5), is shown in Fig. 3, and the parameters of the system are presented in Table I. The analog filter H is a first-order low-pass filter with a time constant τ_v. The DSC uses the present sample and a sample delayed a period T_{DSC} in order to selectively filter the second harmonic. The computation delay is $T_s/6$ and the equivalent ZOH delay is $T_s/2$, where T_s is the voltage regulation sampling time. The blocks *DSC* and *D* are modeled in s-domain by applying Padé approximation with an order as high as required to maintain accuracy [11]. For the power closed-loop G_{cl}, a second-order transfer function is used, where the natural frequency ω_n is related to the current control crossover frequency and the damping ζ_i to its phase margin. The block *C* represents the PI controller, whose parameters are calculated assuming that the PV generator has no influence or is operating at the MPP ($g_t = 0$).

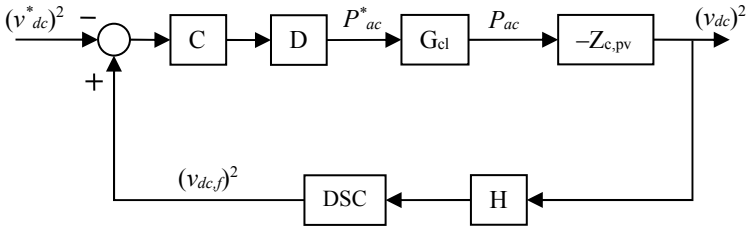

Fig. 3: Control loop for the conventional voltage regulation, including PV array influence.

Table I: Parameters of the system.

Inverter rated power	1110 kVA	Switching frequency, f_{sw}	3 kHz
Grid voltage	400 V	Sampling time, T_s	1 ms
Grid frequency	50 Hz	DSC filter period, T_{DSC}	5 ms
Maximum dc current, $I_{sc,max}$	2000 A	Time constant of the dc voltage filter, τ_v	169 µs
Minimum dc voltage, $V_{dc,min}$	580 V	Crossover frequency of the voltage loop, f_c	15 Hz
Minimum total conductance, $g_{t,min}$	– 3.4 S	Phase margin for the voltage loop	45º
Maximum total conductance, $g_{t,max}$	30 S	Gain of the PI controller, K_P	0.669
PV generator open-circuit voltage in STC	760 V	Time constant of the PI controller, T_n	25.1 ms
PV generator MPP voltage in STC	620 V	Input capacitance, C_{dc}	15 mF
PV generator MPP current in STC	1895 A		

As recommended in the literature, the worst-case RHP pole frequency should be lower than the crossover frequency [9], where a general factor of k_{RHP} is here considered, i.e. $\omega_p < \omega_c/k_{RHP}$. From this condition, (5) and (6), the following constraint for the input capacitance is determined:

$$\omega_{p,\max} = -\frac{g_{t,\min}}{C_{dc}} = \frac{I_{sc,\max}}{C_{dc} \cdot V_{dc,\min}} < \frac{\omega_c}{k_{RHP}} \quad \Rightarrow \quad \frac{C_{dc}}{I_{sc,\max}} > \frac{k_{RHP}}{V_{dc,\min} \cdot \omega_c}. \tag{7}$$

For the case study and considering $k_{RHP} = 2$, a value of 73.2 mF is required for the input capacitor in order to assure stability in every operating point. Since this capacitance is too high, it is decided to reduce its value to 15 mF, i.e. 5 times, in order to decrease the total inverter cost. After this reduction, the conventional control is expected to become unstable in some operating points.

Figure 4 shows the Bode plot of the compensated open-loop transfer function for three operating points: at open-circuit with $g_t = g_{t,max} = 30$ S, at MPP ($g_t = 0$), and below MPP with $g_t = g_{t,min} = –3.4$ S. As can be observed, at MPP the control performance are as designed, with a crossover frequency $f_c = 15$ Hz and a phase margin $PM = 45º$. However, for operating points below MPP, with $g_t < 0$, the phase margin is reduced, which leads to an unstable control for $g_t = g_{t,min} = –3.4$ S.

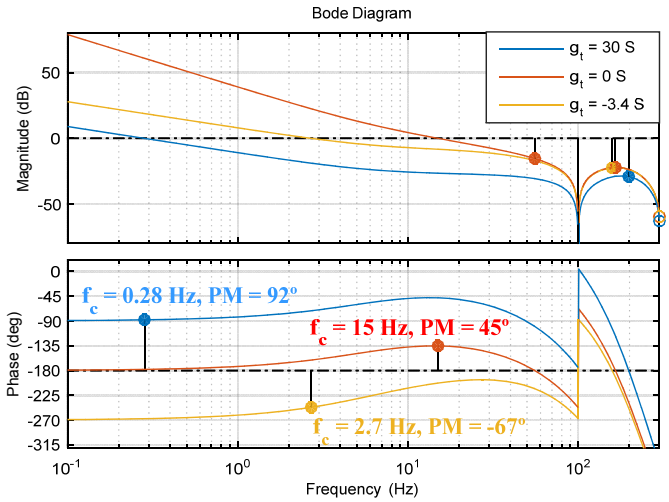

Fig. 4: Compensated open-loop of the conventional voltage regulation, for three operating points.

The conventional voltage regulation is simulated with the PSIM software. The results are shown in Fig. 5 for steps in the voltage reference, where the following variables are represented: dc voltage, reference dc voltage, active power injected to the grid, reference active power and PV total conductance g_t. As can be observed, the control is slow near open-circuit (left graph), becomes faster for MPP with $g_t = 0$ (right graph) and then unstable as soon as the voltage goes below MPP, with $g_t < 0$ (right graph). This results are in agreement with the theoretical model, which predicts an unstable control for $g_t \leq -1$ S, corresponding to $V_{dc} \leq 609$ V.

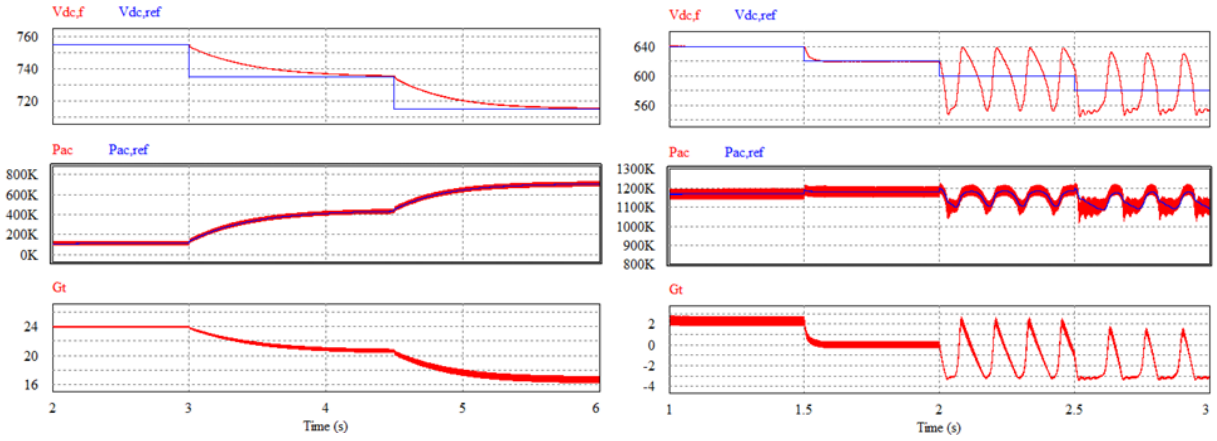

Fig. 5: Simulation results for the conventional voltage regulation.

4. Voltage Regulation with Virtual Impedance Emulation

With the purpose of removing the system RHP pole, an impedance could be included in parallel with the PV generator. To virtually implement this impedance in the digital control, the proposed voltage regulation scheme is shown in Fig. 6, where Y_v is the virtual admittance, P_{Zv} is the power flowing through the virtual impedance/admittance, and $P^*_{ac,v}$ is the controller output or virtual power. As a result of the impedance emulation, the transfer function seen by the controller becomes

$$Z_{eq}(s) = -\frac{\hat{v}_{dc}^2}{\hat{P}_{ac,v}} = \frac{D \cdot G_{cl} \cdot Z_{c,pv}}{1 + D \cdot G_{cl} \cdot Z_{c,pv} \cdot H \cdot DSC \cdot Y_v}. \quad (8)$$

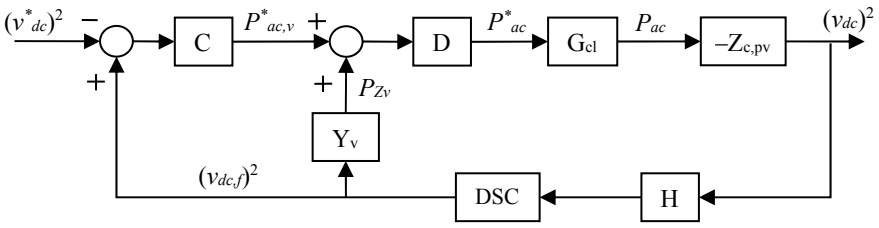

Fig. 6: Control loop for the proposed voltage regulation.

At low frequencies, assuming perfect emulation ($D = G_{cl} = H = DSC = 1$), the controller sees the virtual impedance $Z_v = 1/Y_v$ in parallel with the real impedance $Z_{c,pv}$. Thus, if a virtual conductance $Y_v = g_v/2$ is selected such that $g_v + g_{t,min} > 0$, ideally the RHP pole from $Z_{c,pv}$ would be removed for all operating points. However, due to the different delays, in reality it is not possible to obtain a stable equivalent impedance Z_{eq} for the entire range. In order to compensate part of these delays, the proposed admittance includes a lead compensator with time constants $\tau_z > \tau_p$, that is

$$Y_v(s) = \frac{g_v}{2} \cdot \frac{\tau_z \cdot s + 1}{\tau_p \cdot s + 1}. \tag{9}$$

To evaluate whether the equivalent impedance Z_{eq} has now RHP poles, the open-loop transfer function of the emulation, $OL_{em}=D \cdot G_{cl} \cdot Z_{c,pv} \cdot H \cdot DSC \cdot Y_v$ (see Fig. 6), is examined. This transfer function is plotted in Fig. 7 for $g_v = 4.2$ S, $\tau_z = 2$ ms, $\tau_p = 0.5$ ms and three different operating points: at open-circuit with $g_t = g_{t,max} = 30$ S, at MPP ($g_t = 0$), and below MPP with $g_t = g_{t,min} = -3.4$ S. The latter case is the most critical since it has one RHP pole in the open-loop due to $Z_{c,pv}$. According to generalized Bode criterion [12], to ensure stability in this operating point, it is sufficient that the -180º phase crossing at 0 Hz is with increasing phase and gain higher than 0 dB, and the other -180º phase crossings are with gain lower than 0 dB. To evaluate the two first conditions, the following simple model of the open-loop is considered, which is exact a 0 Hz [12]:

$$OL_{em}(s) = D(s) \cdot G_{cl}(s) \cdot Z_{c,pv}(s) \cdot H(s) \cdot DSC(s) \cdot Y_v(s), \tag{10}$$

$$OL_{em}(s) \approx \frac{1}{\left(\frac{T_s}{2} + \frac{T_s}{6}\right) \cdot s + 1} \cdot \frac{1}{\frac{s^2}{\omega_n^2} + 2\zeta_i \cdot \frac{s}{\omega_n} + 1} \cdot \frac{2}{C_{dc} \cdot s + g_{t,\min}} \cdot \frac{1}{\tau_v \cdot s + 1} \cdot \frac{1}{\frac{T_{DSC}}{2} \cdot s + 1} \cdot \frac{g_v}{2} \cdot \frac{\tau_z \cdot s + 1}{\tau_p \cdot s + 1}. \tag{11}$$

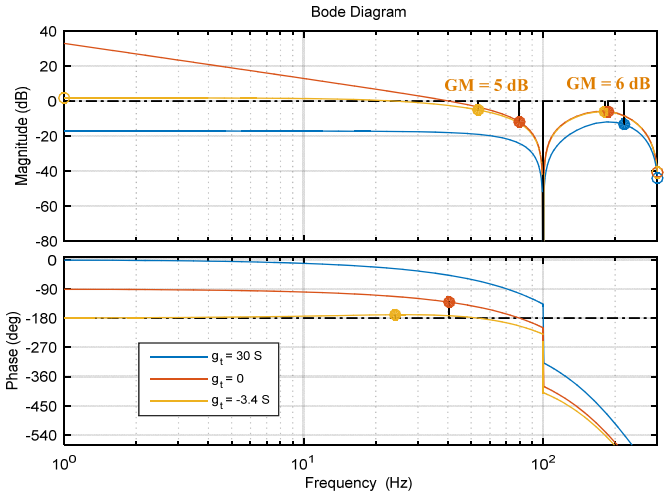

Fig. 7: Open-loop of the impedance emulation, OL_{em}, for three operating points.

From (11), the condition to achieve an open-loop gain at 0 Hz higher than 0 dB is

$$\left|OL_{em}(j\omega=0)\right| = \frac{2}{\left|g_{t,\min}\right|}\cdot\frac{g_v}{2} > 1 \quad \Rightarrow \quad g_v > \left|g_{t,\min}\right|. \tag{12}$$

Similarly, the condition to attain an open loop with increasing phase at 0 Hz becomes

$$\left.\frac{dPhase\left[OL_{em}(j\omega)\right]}{d\omega}\right|_{\omega=0} = -\frac{T_s}{2}-\frac{T_s}{6}-\frac{2\zeta_i}{\omega_n}+\frac{C_{dc}}{\left|g_{t,\min}\right|}-\tau_v-\frac{T_{DSC}}{2}+\tau_z-\tau_p \geq 0, \tag{13}$$

$$\tau_z-\tau_p \geq \frac{T_s}{2}+\frac{T_s}{6}+\frac{2\zeta_i}{\omega_n}+\tau_v+\frac{T_{DSC}}{2}-\frac{C_{dc}}{\left|g_{t,\min}\right|}. \tag{14}$$

Selecting the aforementioned impedance parameters, $g_v = 4.2$ S, $\tau_z = 2$ ms, $\tau_p = 0.5$ ms, both conditions (12) and (14) are fulfilled with certain margins and thus the equivalent impedance Z_{eq} has no RHP. This impedance is shown in Fig. 8 for the three previous operating points. It can be observed that, at low frequencies, it behaves as the PV total conductance g_t in parallel with the virtual conductance g_v. The PI controller is then designed to achieve a crossover frequency $f_c = 15$ Hz and a gain margin GM = 7 dB for $g_{t,min} = -3.4$ S. With this controller, the open-loop transfer function is represented in Fig. 9 for the three previous operating points. As can be observed, the control performance is as designed for $g_{t,min} = -3.4$ S and becomes slower for other operating points. In any case, thanks to the proposed method, the control is fast and stable for all operating points after a drastic capacitance reduction.

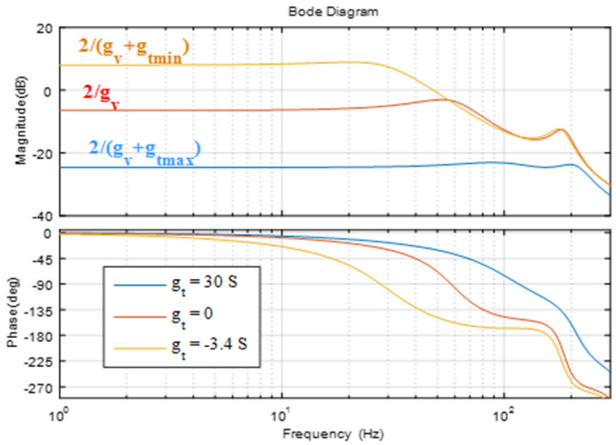

Fig. 8: Equivalent impedance, Z_{eq}, for three operating points.

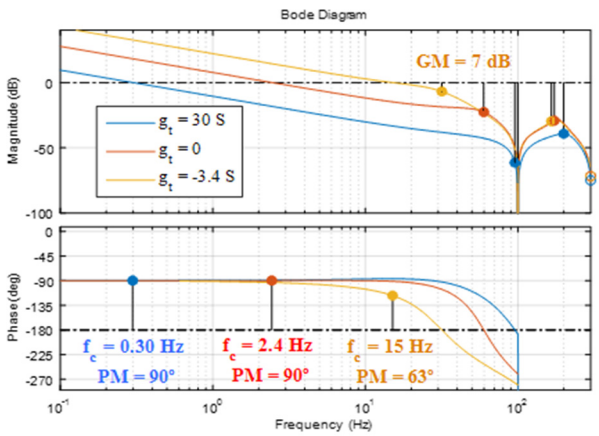

Fig. 9: Compensated open-loop of the proposed voltage regulation, for three operating points.

The proposed voltage regulation is validated by simulation for the same conditions as for the conventional voltage regulation. As can be observed in Fig. 10, near open-circuit (left graph) the control is slow, in the same way as for the conventional control (see Fig. 5). However, when the voltage is around or below MPP voltage (right graph), the control is fast and stable. In short, the proposed method achieves an adequate regulation for the whole operating range after a large capacitance reduction.

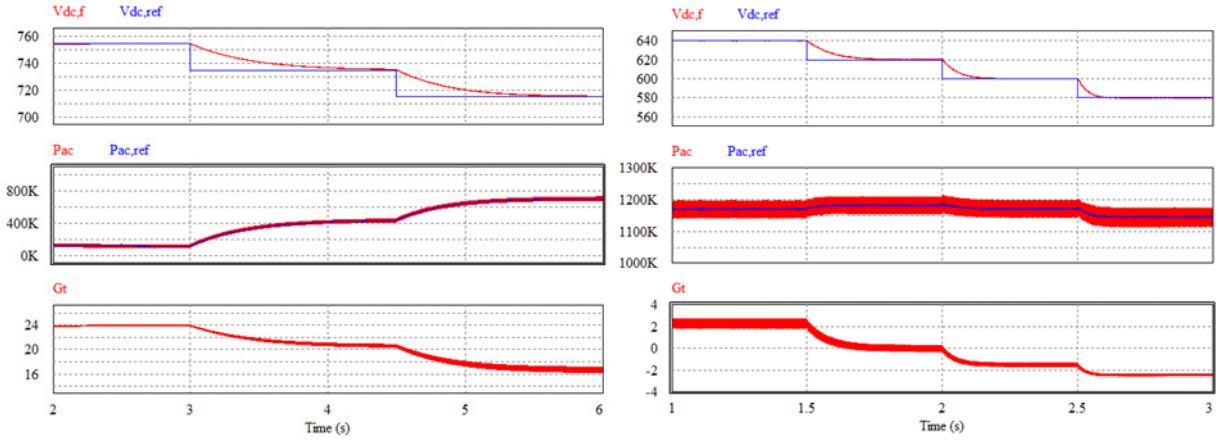

Fig. 10: Simulation results for voltage regulation with virtual impedance emulation.

5. Conclusions

This paper analyzes the voltage regulation in grid-connected three-phase PV inverters. It is first shown that, due to the PV generator influence, a RHP pole appears when the operating voltage is below MPP. As a result, the conventional control requires a large capacitor in order to guarantee stability in the whole operating range. Then, to reduce this capacitance, a voltage regulation which emulates a virtual impedance in parallel with the PV generator is proposed. The emulation removes the RHP pole from the plant seen by the voltage controller, making it possible to achieve an adequate voltage regulation in all operating points with a smaller capacitor. Simulation results validate the analysis, showing that the control is fast and stable after reducing the capacitance by a factor of 5.

References

[1] "Renewables 2018 global status report," REN21, 2018.

[2] J. C. Giacomini, L. Michels, H. Pinheiro, and C. Rech, "Active damping scheme for leakage current reduction in transformerless three-phase grid-connected PV inverters," *IEEE Transactions on Power Electronics*, vol. 33, no. 5, pp. 3988-3999, 2018.

[3] M. A. Shuvra, B. Chowdhury, "Distributed dynamic grid support using smart PV inverters during unbalanced grid faults," *IET Renewable Power Generation*, vol. 13, no. 4, pp. 598-608, 2019.

[4] R. Kadri, J. Gaubert, and G. Champenois, "An improved maximum power point tracking for photovoltaic grid-connected inverter based on voltage-oriented control," *IEEE Transactions on Industrial Electronics*, vol. 58, no. 1, pp. 66-75, 2011.

[5] A. Urtasun, P. Sanchis, and L. Marroyo, "Adaptive voltage control of the dc/dc boost stage in PV converters with small input capacitors," *IEEE Transactions on Power Electronics*, vol. 28, no. 11, pp. 5038-5048, 2013.

[6] A. Urtasun, J. Samanes, E. L. Barrios, P. Sanchis, and L. Marroyo, "Control of a photovoltaic array interfacing current-mode-controlled boost converter based on virtual impedance emulation," *IEEE Transactions on Industrial Electronics*, vol. 66, no. 5, pp. 3496-3506, 2019.

[7] M. G. Villalva, T. G. Siqueira, and E. Ruppert, "Voltage regulation of photovoltaic arrays: small-signal analysis and control design," *IET Power Electronics*, vol. 3, no. 6, pp. 869-880, 2010.

[8] T. Messo, J. Jokipii, and T. Suntio, "Minimum dc-link capacitance requirement of a two-stage photovoltaic inverter," in *2013 IEEE Energy Conversion Congress and Exposition*, pp. 999-1006, 2013.

[9] S. Skogestad, I. Postlethwaite, "Multivariable feedback control: Analysis and design," John Wiley & Sons Ltd., West Sussex, England, 1996.

[10] T. Messo, J. Jokipii, J. Puukko, and T. Suntio, "Determining the value of dc-link capacitance to ensure stable operation of a three-phase photovoltaic inverter," *IEEE Transactions on Power Electronics*, vol. 29, no. 2, pp. 665-673, 2014.

[11] J. Samanes, A. Urtasun, E. Gubia, and A. Petri, "Robust multisampled capacitor voltage active damping for grid-connected power converters," *Electrical Power and Energy Systems*, vol. 105, pp. 741-752, 2019.

[12] D. Lumbreras, E. L. Barrios, A. Urtasun, A. Ursúa, L. Marroyo, and P. Sanchis, "On the stability of advanced power electronic converters: the generalized Bode criterion," *IEEE Transactions on Power Electronics*, DOI 10.1109/TPEL.2018.2884892, early access.